The electrical and optical measurements were performed after the laser definition step, to test the uniformity of the device. All the measurements were performed at room temperature without heat sinking using a pulsed current source (200 ns pulse width, 10 kHz repetition rate). Light was coupled out from the array through the substrate side.

Light output against injection current was measured for all the VCSELs of the array (Fig. 3). The results are summarised in Figs. 4*a* and *b*. All the 1024 lasers were operating with a most probable (MP) threshold current of 6·8 mA and MP output differential quantum efficiency (DQE) of 8%. The spread is about 18% for the threshold current and about 30% for the DQE. The spatial lasing mode characteristics were measured by imaging the lasing near (NF) and far (FF) field distributions on a video imager (inset of Fig. 3). The results of the measurements on 49 lasers regularly sampled over the array are summarised in Fig. 4*c*. The lasers are lasing in a single spatial mode for a current range exceeding twice the threshold current. The measured lasing NF full width at half maximum (FWHM) is 11 μm and the FF angular FWHM is 4·6°, indicating lasing in a diffraction limited TEM_{00} Gaussian spatial mode.

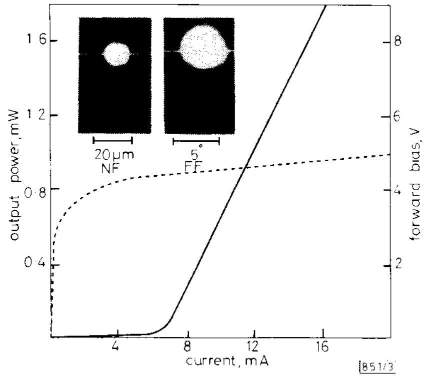

Fig. 3 *Typical light output and operating voltage against current of laser of array*

Typical near field and far field distributions depicted in inset

——— typical light output

– – – – operating voltage

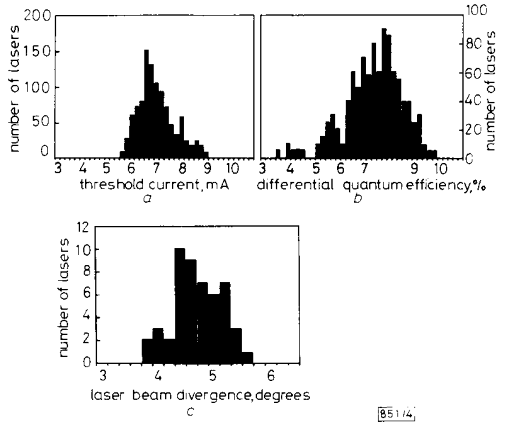

Fig. 4 *Properties of MASELA measured after laser definition step*

a Distribution of threshold currents of all lasers in array

b Distribution of quantum differential efficiency of all lasers in array

c Distribution of angular beam spread of 50 lasers of array, measured at current level of 10 mA (~ 1·5 × $i_{threshold}$)

The electrical performance measurements are summarised here. The resistance of each of the n^+ columns (top to bottom) is 240 Ω. The intercolumn isolation resistance is better than 0·5 MΩ. The current against voltage measurements on 50 lasers showed a mean series resistance of 28 Ω (Fig. 3). The threshold voltage, was 3·8–5 V, depending of the distance between the laser and its n^- contact pad. Finally, the matrix addressing was verified by randomly activating lasers by selecting their row and column terminals.

In summary, an integrated 2-D array of a 1024 vertical cavity surface emitting laser array was successfully fabricated and tested. The electrical and optical characteristics of the lasers were found to be fairly homogeneous over the array area. The array architecture, based on matrix addressing scheme enables easy and fast electrical access to each of the lasers in the array, as was demonstrated in our preliminary addressing experiments.

Acknowledgment: This work was partially supported by US Army Electronics Technology and Devices Laboratory, Contract DAAL01-89-C-0900.

M. ORENSTEIN
A. C. VON LEHMEN
C. CHANG-HASNAIN
N. G. STOFFEL
J. P. HARBISON
L. T. FLOREZ

Bellcore
331 Newman Springs Road
Red Bank, NJ 07701, USA

2nd January 1991

References

1 SODA, H., IGA, K., KITAHARA, C., and SUEMATSU, Y.: 'GaInAsP/InP surface emitting injection lasers', *Jpn. J. Appl. Phys.*, 1979, **18**, pp. 2329–2330

2 GEELS, R. S., and COLDREN, L. A.: 'Submilliamp threshold vertical-cavity laser diodes', *Appl. Phys. Lett.*, 1990, **57**, pp. 1605–1606

3 SCHERER, A., JEWELL, J. L., LEE, Y. H., HARBISON, J. P., and FLOREZ, L. T.: 'Fabrication of microlasers and microresonator optical switches', *Appl. Phys. Lett.*, 1989, **55**, pp. 2724–2726

4 PAEK, E. G., WULLERT II, J. R., JAIN, M., VON LEHMEN, A., SCHERER, A., HARBISON, J., FLOREZ, L. T., YOO, H. J., MARTIN, R., JEWELL, J. L., and LEE, Y. H.: 'Compact and ultrafast holographic memory using a surface-emitting microlaser diode array', *Opt. Lett.*, 1990, **15**, pp. 341–343

5 UCHIYAMA, S., and IGA, K.: 'Two-dimensional array of GaInAsP/InP surface emitting lasers', *Electron. Lett.*, 1985, **21**, pp. 162–164

6 LEE, Y. H., JEWELL, J. L., SCHERER, A., MCCALL, S. L., HARBISON, J. P., and FLOREZ, L. T.: 'Room temperature continuous-wave vertical-cavity single-quantum-well microlaser diodes', *Electron. Lett.*, 1989, **25**, pp. 1377–1378

7 VON LEHMEN, A., CHANG-HASNAIN, C., WULLERT II, J. R., CARRION, L., FLOREZ, L. T., and HARBISON, J. P.: 'Independently addressable VCSE laser array' (submitted for publication)

8 ORENSTEIN, M., VON LEHMEN, A. C., CHANG HASNAIN, C., STOFFEL, N. G., HARBISON, J. P., FLOREZ, L. T., and CLAUSEN, E.: 'Vertical-cavity surface-emitting InGaAs/GaAs lasers with planar lateral definition', *Appl. Phys. Lett.*, 1990, **56**, pp. 2384–2386

CODING TO ALLEVIATE INTERMODULATION DISTORTION IN COHERENT OPTICAL FSK SINGLE-OCTAVE SCM SYSTEMS

Indexing terms: Optical communications, Multiplexing, Codes and coding

For a coherent optical single-octave SCM system, the number of channels that can be located within a given optical band is a major concern. A theoretical analysis of the FSK single-octave SCM system employing Reed-Solomon codes to increase the number of channels is presented. The example shows that by using a (256, 192) rate 3/4 Reed-Solomon code, the number of channels can be increased threefold and the influence of intermodulation distortion can also be greatly reduced.

Introduction: Recently, research on optical fibre communications employing subcarrier multiplexed (SCM) microwave carriers has been focused on the transmission of large numbers of digital channels using coherent techniques.[1] For a coherent SCM system, the intermodulation distortion (IMD) is a fundamental characteristic of the modulation/detection process and therefore imposes a limit on the obtainable receiver sensitivity; from another point of view, for a given receiver sensitivity, the number of channels is restricted. We theoretically investigate the benefit of applying coding to a coherent optical frequency-shift-keying (FSK) single-octave SCM system. A general expression of the number of channels N is derived in terms of carrier-to-noise ratio (CNR), receiver sensitivity, and code parameters. It is shown that coding can be used to effectively alleviate the impact of IMD; thus more channels can be located into a specific optical band.

System description and analysis: Fig. 1 shows a schematic diagram of a coherent SCM system with N channels. When the channel crosstalk is negligible and the local oscillator (LO) power is large enough to suppress thermal noise, the CNR of channel i is given as[1]

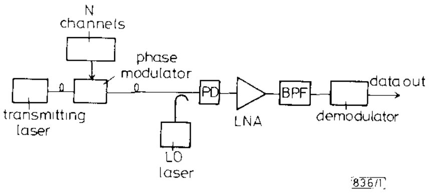

Fig. 1 *Coherent optical subcarrier multiplexed system*

$$\rho = \frac{A\beta^2}{2eRP_{LO}B_{IF} + h_3 k_3(i) A\beta^6/16} \tag{1}$$

where $A = 0{\cdot}5R^2 P_{LO} P_S$, R is the responsivity, P_{LO} is the LO power, P_S is the received signal power, e is the electron charge, β is the phase modulation (PM) index, B_{IF} is the bandwidth of the IF filter, the factor h_3 represents the fraction of the IMD power that passes through the IF filter and equals 2/3 for a ideal rectangular signal spectrum, and $k_3(i)$ is the number of IMD and can be expressed as

$$k_3(i) = \frac{i(N-i+1)}{2} + \frac{[(N-3)^2-5]}{4} \tag{2}$$

For a single-octave SCM system, every channel has almost the same performance in our analysis. In the following derivations, we consider the CNR of the central channel ($i = (N+1)/2$), which has the most IMD as the criterion; thus $k_3((N+1)/2)$ is $(3N^2 - 10N + 9)/8$.

For the uncoded case, from eqns. 1 and 2, the CNR of the central channel can be obtained as

$$\rho = \frac{A\beta^2}{2eRP_{LO}B_{IF} + A\beta^6(N^2 - \frac{10}{3}N + 3)/64} \tag{3}$$

With simple algebraic manipulation, we obtain

$$N^2 - \frac{10}{3}N + 3 = 64\left(\frac{1}{\rho\beta^4} - \frac{4eB_{IF}}{RP_S\beta^6}\right) \tag{4}$$

Note that the left side of eqn. 4 is a monotonically increasing function of N when $N > 5/3$, which is the case of practical interest. We can thus maximise N by optimising β, when P_s and ρ are fixed.[2] Differentiating the right hand side of eqn. 4 with respect to β and set to zero, the following is obtained:

$$\beta_{opt} = \sqrt{\left(\frac{6eB_{IF}\rho}{RP_S}\right)} \tag{5}$$

Therefore, for an uncoded system, the maximum value of N is

$$N_{uncoded} = \sqrt{\left(\frac{16}{27}\right)\frac{RP_S}{eB_{IF}}\rho^{-3/2}} + \frac{5}{3} \tag{6}$$

For the coded case, the parameter E_b/N_0 may be used as a measure of system quality instead of CNR, where E_b is the energy per bit and N_0 is the height of the (white) noise power spectrum. We assume that the CNR can be approximated as E_b/N_0 in following analysis.[1]

Suppose the noise is Gaussian distributed and a code of rate r is used for which the coding gain is G. The required CNR becomes ρ/G. Hence, eqn. 3 can be modified as

$$\frac{\rho}{G} = \frac{A\beta^2}{2eRP_{LO}B_{IF}/r + A\beta^6(N^2 - \frac{10}{3}N + 3)/64} \tag{7}$$

Substituting eqn. 5 into eqn. 7 and solving for N

$$N_{coded} = \sqrt{\left(\frac{16}{9}G - \frac{32}{27r}\right)\frac{RP_S}{eB_{IF}}\rho^{-3/2}} + \frac{5}{3} \tag{8}$$

Numerical example: We assume a 100 Mbit/s FSK system requiring a bit error rate (BER) of 10^{-9} and adopt the following parameters:[1] $\rho = 18$ dB, $R = 1$ A/W, $B_{IF} = 120$ MHz, and $P_S = -40$ dBm; therefore, from eqn. 5, $\beta_{opt} = 0{\cdot}27$. The code rate r is chosen to be in the interval $B_{IF}/D \leq r \leq 1$, where D is the channel spacing and is assumed to be 200 MHz.[1] Therefore, r must be larger than 0·6 to avoid significant degradation from adjacent channel crosstalk. By substituting the above parameters into eqn. (6) we obtain $N_{uncoded} = 9$. By using a (256, 192) rate 3/4 Reed-Solomon code with a coding gain of 6·3 dB[2,3] ($G = 10^{0{\cdot}63}$ and $r = 3/4$) in eqn. 8, we obtain $N_{coded} = 27$. Fig. 2 shows the number of channels against received signal power for the coded system and the uncoded system at CNR = 18 dB. It is found that the channel number can be increased threefold under the same receiver sensitivity and BER.

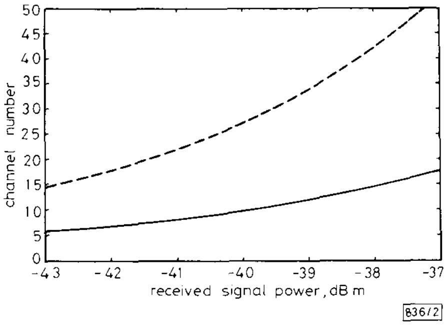

Fig. 2 *Number of channels against received signal power for (256, 192) Reed-Solomon coded and uncoded system at CNR = 18 dB*

- - - - N coded
——— N uncoded

Conclusion: A general expression of a coherent optical single-octave SCM system employing error control code to increase the number of channels is derived in terms of received signal power, carrier-to-noise ratio, and code parameters. As an example, by using a (256, 192) Reed-Solomon code in a coherent optical FSK single-octave SCM system, the number of channels can be increased threefold. Therefore, coding can be used to effectively combat intermodulation distortion, and more channels can be located within an optical band.

J. H. WU
J. WU
Y.-H. LEE

Department of Electrical Engineering
National Taiwan University
Taipei, Taiwan, 10764, Republic of China

2nd January 1991

References

1 GROSS, R., and OLSHANSKY, R.: 'Multichannel coherent FSK experiment using subcarrier multiplexing techniques', *J. Lightwave Technol.*, 1990, **8**, (3), pp. 406–415

2 FOSCHINI, G. J., and SALEH, A. A. M.: 'Overcoming optical amplifier intermodulation distortion using coding in multichannel communications systems', *IEEE Trans. Commun.*, 1990, **38**, (2), pp. 187–191

3 BERLEKAMP, E. R., PELIE, R. E., and POPE, S. P.: 'The application of error control to communications', *IEEE Commun. Mag.*, April 1987, **25**, pp. 44–56

ELECTRICAL PROPERTIES OF THIN OXYNITRIDED SiO_2 FILMS FORMED BY RAPID THERMAL PROCESSING IN AN N_2O AMBIENT

Indexing terms: Thin films, Metal-oxide-semiconductor structures, Annealing

The optimisation of reaction temperature and time has been made in the oxynitridation of SiO_2 in N_2O by evaluating its dielectric properties at a constant current stress. It is found that N_2O-oxynitrided SiO_2 films are much improved in both charge trapping density and charge to breakdown when the optimum oxynitridation process (O_2, 1100°C, 5 s and following N_2O, 1200°C, 25 s) is chosen.

In the near future, the preparation of highly reliable thin (< 10 nm) SiO_2 films becomes one of the critical factors in realising deep sub-0·5 μm MOSFETs and scaled nonvolatile memories such as EPROMs and EEPROMs. In the last decade, thermal nitridation of SiO_2 films in NH_3 has been studied as an alternative for gate and tunnelling insulators because of the reliability problem of thin SiO_2 film.[1,2] To improve long-term reliability of thin SiO_2 film, reoxidation of NH_3-nitrided SiO_2 film has attracted much attention.[3–5] We have recently achieved for the first time a method of forming highly reliable nitrided SiO_2 without NH_3.[6,7] This process consists of the combination of *in situ* oxidation with O_2 followed by *in situ* oxynitridation with nitrous oxide (N_2O) by rapid thermal processing (RTP). By this process nitrogen of about 5 atomic % can be introduced at the SiO_2/Si interface. These N_2O-oxynitrided SiO_2 (SiO_xN_y) films show smaller changes in interface trap states and lower charge trapping densities as compared to those of pure SiO_2 films. As a result, a large charge-to-breakdown value ($> 30\,C/cm^2$) under the condition of negatively-biased gate can be achieved.

The purpose of this work is to examine the detailed correlations between electrical properties and oxynitridation conditions. It will be demonstrated that by proper nitridation, the dielectric reliability of thin gate SiO_2 films can be greatly improved.

SiO_2 and SiO_xN_y films were formed on 3–5 Ω cm, *p*-type (100) Si, 5 inch wafers after the standard cleaning procedure reported elsewhere.[7] Dielectric films were formed in an RTP chamber equipped with tungsten–halogen lamp heaters and with an oil-free high-vacuum pumping system. Table 1 shows the process sequences employed. The total film thickness was defined to be the sum of the first thickness (T_{ox1}) after oxidation thickness (T_{ox2}) after oxynitridation. For all samples, the total film thicknesses ($= T_{ox1} + T_{ox2}$) were controlled to be 10 nm ± 0·3 nm. MOS capacitors were fabricated by depositing n^+ polysilicon films and by delineating the polysilicon films to have an area of $2 \times 10^{-4}\,cm^2$ on the dielectric films. To determine the time-dependent-dielectric-breakdown (TDDB) characteristics of SiO_2 and SiO_xN_y films, electrons were injected, in the Fowler–Nordheim (F–N) region, from the gate electrode into the dielectric film at a constant current density ($J_{ox} = -100\,mA/cm^2$). High-frequency (1 MHz) capacitance/voltage (C/V) measurement was used to monitor flatband voltage (V_{FB}) in high-field stressing.

Table 1 PREPARATION SEQUENCES EMPLOYED

Sample number	*RTO*	*RTON*	T_{ox1}	T_{ox2}
			nm	nm
RTO-68	O_2, 1100°C, 28 s	—	10	0
RTON-11	O_2, 1100°C, 22 s	N_2O, 1100°C, 3 s	9	1
RTON-12	O_2, 1100°C, 17 s	N_2O, 1100°C, 20 s	8	2
RTON-13	O_2, 1100°C, 12 s	N_2O, 1100°C, 45 s	7	3
RTON-14	O_2, 1100°C, 22 s	N_2O, 1200°C, 1 s	9	1
RTON-15	O_2, 1100°C, 17 s	N_2O, 1200°C, 3 s	8	2
RTON-16	O_2, 1100°C, 12 s	N_2O, 1200°C, 10 s	7	3
RTON-17	O_2, 1100°C, 5 s	N_2O, 1200°C, 25 s	5	5

Gate voltage shifts, ΔV_g, at constant current density are plotted in Fig. 1. The ratio, $T_{ox2}/(T_{ox1} + T_{ox2})$, is taken as a parameter. For pure SiO_2 (control), V_g is greatly shifted to the positive direction at the initial stage, and then increased almost linearly to the negative direction with increasing injected charge, $Q_{inj}(= J_{ox} \cdot t)$. On the contrary, for the SiO_xN_y films, the amounts of positive V_g shifts, $V_{gs(max)}$, are smaller than that of pure SiO_2. Both $V_{gs(max)}$ and the slope in the negative ΔV_g range, dV_g/dQ_{inj}, become smaller with increasing the ratio, $T_{ox2}/(T_{ox1} + T_{ox2})$.

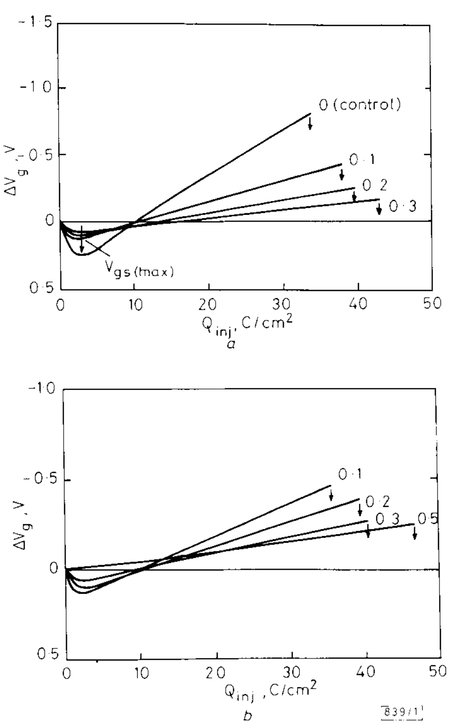

Fig. 1 *Gate voltage shift against injected charge*

$T_{ox2}/(T_{ox1} + T_{ox2})$
a T_{O_2} = 1100°C T_{N_2O} = 1100°C
b T_{O_2} = 1100°C T_{N_2O} = 1200°C

Fig. 2 shows the effect of the ratio, $T_{ox2}/(T_{ox1} + T_{ox2})$ on $V_{gs(max)}$ and $dV_g/dF(= q \cdot dV_g/dQ_{inj})$, where electron fluence is denoted by F. As is well known, $V_{gs(max)}$ corresponds to the hole trap generation.[8] Conversely, dV_g/dF corresponds to the rate of electron trap generation.[9] As Fig. 2 shows, the tendency of $V_{gs(max)}$ on preparation conditions is close to that of dV_g/dF. Thus, it is noted that electron traps are generated to cancel the generated positive charge during high-field stressing. As seen in Fig. 2, the values, $V_{gs(max)}$ and dV_g/dF, can reduce with increasing the ratio, $T_{ox2}/(T_{ox1} + T_{ox2})$ in both the oxynitridation temperatures, 1100°C and 1200°C.

The effect of oxynitridation conditions on ΔV_{FB} after $2\,C/cm^2$ injection and charge to breakdown, Q_{BD}, are shown in Fig. 3. The amount of ΔV_{FB} corresponds to the density of hole traps. Therefore, the effect of the ΔV_{FB} on preparation conditions is similar to that of $V_{gs(max)}$ shown in Fig. 2. As ΔV_{FB} decreases, which corresponds to the reduction of charge